Composites Part B 163 (2019) 431–437

Contents lists available at ScienceDirect

Composites Part B

journal homepage: www.elsevier.com/locate/compositesb

Simultaneous enhancement of mechanical and electrical properties of carbon nanotube fiber by infiltration and subsequent carbonization of resorcinol-formaldehyde resin

Young-Jin Kim[a,b], Junbeom Park[a], Hyungjun Kim[c], Hyeon Su Jeong[a], Joong Hee Lee[b], Seung Min Kim[a], Young-Kwan Kim[a,*]

[a] Carbon Composite Materials Research Center, Korea Institute of Science and Technology, 92 Chudong-ro, Bongdong-eup, Wanju-gun, Jeonbuk, 55324, Republic of Korea
[b] Department of BIN Fusion Technology, Chonbuk National University, Duckjindong 1Ga 664-14, Jeonju, Jeolabuk-do, 561-756, Republic of Korea
[c] Department of Chemistry, Incheon National University, 119 Academy-ro, Yeonsu-gu, Incheon, 22012, Republic of Korea

ARTICLE INFO

Keywords:
Carbon-carbon composites (CCCs)
Fibres
Mechanical properties
Electrical properties
Heat treatment

ABSTRACT

An efficient strategy to enhance mechanical and electrical properties of carbon nanotube (CNT) fiber is developed by using resorcinol-formaldehyde (RF) resin as a functional infiltrating agent that can be carbonized under a mild condition. This strategy is a sequential process including infiltration of RF resin into CNT fiber, thermal stabilization and carbonization. The selection of resin and additive, and enhancement mechanism are elucidated by theoretical and experimental approaches. By using this strategy, the tensile strength, modulus, specific tensile strength and electrical conductivity of CNT fiber are enhanced by 8.2, 16.4, 2.1 and 3.6 fold, respectively.

1. Introduction

The macroscopic assembly of carbon nanotube (CNT) into fibrous form is an urgent issue to improve its processibility for automobile, defense and aerospace industries while maintaining their fascinating intrinsic mechanical and electrical properties [1,2]. Several spinning techniques have been developed such as forest spinning from vertically grown carpet of CNT on a substrate [3], liquid crystal spinning from concentrated CNT in strong acids [4], and direct spinning of CNT synthesized from chemical vapor deposition (CVD) reactor with floating catalysts [5,6]. Among those techniques, the direct spinning has been considered as a promising strategy based on its scale-up and continuous production potential.

The direct spinning produces CNT fibers with lower mechanical and electrical properties than individual CNT, and their inferior properties originated from loosely-packed structures [7]. For reinforcement of CNT fibers, the densification processes have been extensively explored with roll-pressing [7], infiltration with liquids [8] or polymers [9], and chemical vapor infiltration [10]. The polymer infiltration is an efficient strategy to densify CNT fibers by filling their voids with polymers as well as improve the load transfer efficiency [9]. Even though the infiltration of polymers such as poly (vinyl alcohol) (PVA) into CNT fibers has shown the promise regarding to their mechanical properties, it resulted in decrease of their electrical conductivity due to their insulating property and increasing contact resistance [11]. Instead, the infiltration of conducting polymers lead to the enhancement of electrical conductivity of CNT fibers, but it negligibly affected their mechanical properties [12].

Ryu et al. recently reported that the mechanical and electrical properties of forest spun CNT fibers were considerably enhanced by infiltration of polydopamine followed by pyrolysis at 1050 °C under H_2 atmosphere for carbonization of polydopamine [13]. This report implied that the infiltration and pyrolysis of carbonizable polymers into CNT fibers can efficiently improve both their mechanical and electrical properties. However, the high-temperature pyrolysis of polymer infiltrated CNT fibers under reductive condition is a highly energy consuming and expensive process, and requires the precisely controlled environment to prevent thermal damage and oxidation of carbon materials [13].

Those features of high-temperature pyrolysis process render the reinforcement process of CNT fibers cumbersome and restricted its potential for a large-scale production. In this regard, the rational selection of infiltrating polymer is a prerequisite for optimizing the reinforcement process of CNT fibers. An optimal infiltrating polymer should provide cost-effectiveness, lightness, strong adhesiveness to CNT fibers and mild carbonization condition. Preliminary density functional theory (DFT) simulations and experimental findings suggest the resorcinol-formaldehyde (RF) can outperform polydopamine: RF is

* Corresponding author.
E-mail address: youngkwan@kist.re.kr (Y.-K. Kim).

https://doi.org/10.1016/j.compositesb.2018.12.132
Received 4 July 2018; Received in revised form 27 December 2018; Accepted 30 December 2018
Available online 02 January 2019
1359-8368/

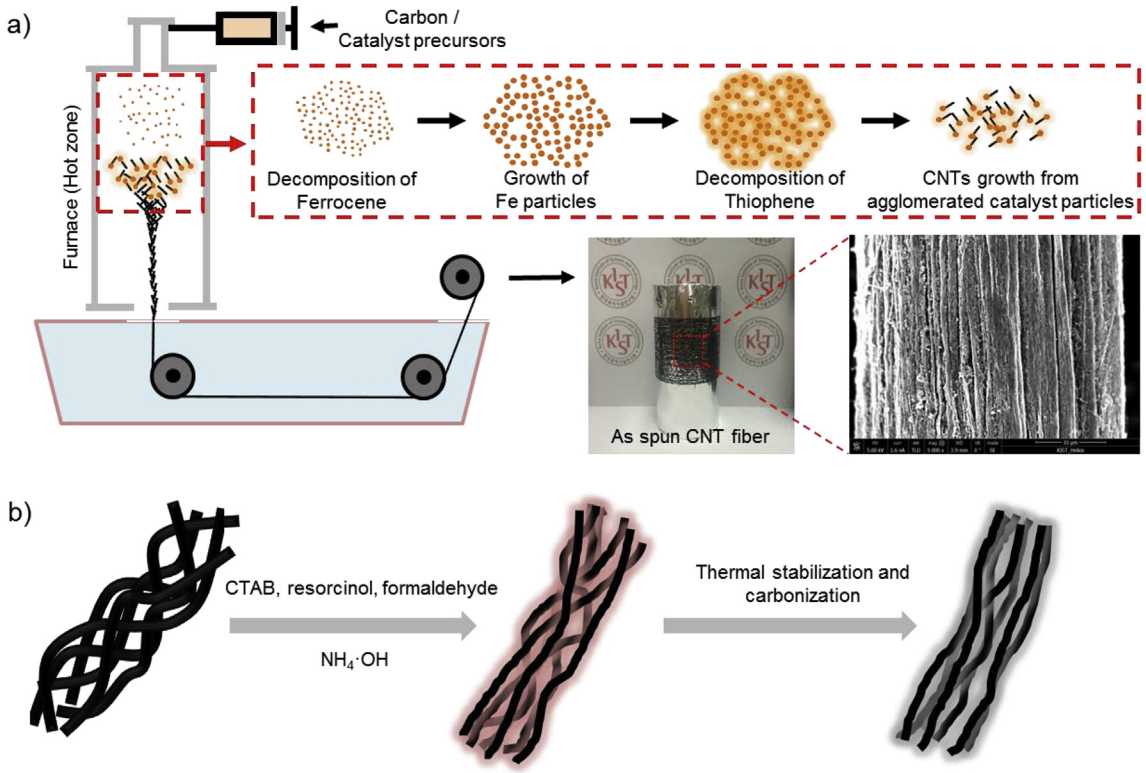

Fig. 1. (a) Fabrication process and photograph of the direct spun CNT fibers. (b) Schematic illustration of RF resin infiltration, thermal stabilization and carbonization of the direct spun CNT fibers.

predicted to bind to CNT stronger than polydopamine does, and RF resin can be carbonized at low-temperature around 600 °C under inert atmosphere. In addition, the carbonized RF resin provides thermal shrinkage, high strength and electrical conductivity that are essential features to improve both mechanical and electrical properties of CNT fibers [14].

Herein, we demonstrate an efficient reinforcing strategy for CNT fibers by using RF resin infiltration followed by thermal stabilization and carbonization (Fig. 1). The selections of a resin and an enhancer are made based on the DFT simulations: RF resin and cetyltrimethylammonium bromide (CTAB). Based on the designed interfacing structures, the CNT fiber infiltrated with RF resin by CTAB (C-RF@CNT fiber) exhibits highly enhanced tensile strength of 244 MPa, specific tensile strength of 0.56 N tex^{-1} and electrical conductivity of 1741 S cm^{-1} compared to those of pristine CNT fiber (tensile strength: 71 MPa, specific strength: 0.42 N tex^{-1} and electrical conductivity: 968 S cm^{-1}) without the thermal treatment which is essentially required for polydopamine-based reinforcement. By the thermal stabilization and carbonization processes, the tensile, specific tensile strength and electrical conductivity of the C-RF@CNT fibers were further enhanced to 610 MPa, 0.86 N tex^{-1} and 3513 S cm^{-1}, respectively. The considerable enhancement of both mechanical and electrical properties of CNT fibers confirmed that the RF resin infiltration, stabilization and carbonization are an efficient strategy for the large-scale production of high-performance CNT fibers, and the plausible enhancement mechanism was demonstrated with theoretical and experimental results.

2. Experimental section

2.1. Preparation of C-RF@CNT fibers

CNT fibers were produced by the previously reported method [5,6]. 75 mg of CTAB was added in 40 mL of the water and ethanol mixture (3:1) containing 182 mg of ammonium hydroxide (25–30 wt%). After stirring for 30 min, 16 mg of resorcinol and 25 mg of formaldehyde were added to the mixture for polymerization. CNT fibers were immersed into the mixture for 3 h, washed by using water and ethanol, and dried under reduced pressure for 3 h.

2.2. Carbonization of C-RF@CNT fibers

C-RF@CNT fibers were stabilized in a muffle furnace at 270 °C for 1 h with 10 °C min^{-1} heating rate under air. The stabilized C-RF@CNT fibers were inserted in a tube furnace, degassed at1 × 10^{-3} torr, and heated to 600 °C with 10 °C/min heating rate for 1 h under Ar flow.

2.3. Tensile experiments

For tensile test, all fibers were cut to 30 mm and analyzed by using a Textechno Favimat using a 0–2 N load cell with a resolution of 10^{-6} N, 20 mm gauge length and 2 mm/min loading rate. The tensile test was repeated at least 10 times for each fiber to obtain statistical values.

2.4. Electrical conductivity measurements

The electrical resistance was measured by using a Keithley2000E with the four-point probes method. The electrical conductivity (S cm^{-1}) of all fibers was calculated through $k = (R \times A/L)^{-1}$, where R, A and L were resistance, cross section area and length of each fiber, respectively. The electrical conductivity was also measured at least 5 times to obtain statistical values.

2.5. DFT simulation

DFT calculation employing ωB97X-D/6-31G* [15] have been performed to find the most thermodynamically stable geometry. All theoretical predictions regarding geometry and total interaction energy have been made using quantum chemistry package Q-Chem 3.0 [16].

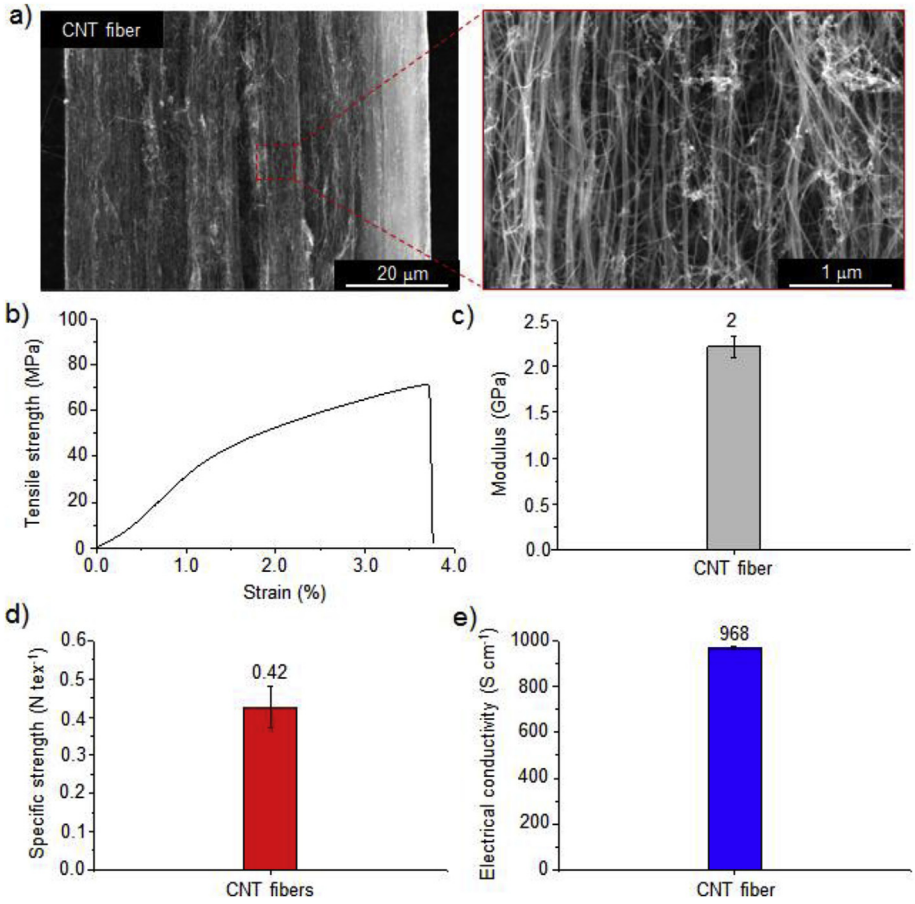

Fig. 2. (a) SEM images, (b) stress and strain curve, (c) modulus, (d) specific tensile strength and (e) electrical conductivity of CNT fibers.

Zeroth-order symmetry-adapted perturbation theory (SAPT0) [17] is employed to characterize the noncovalent interaction as the sum of electrostatic, exchange, induction, and dispersion terms. The geometries obtained at the DFT simulations are taken, and correlation-consistent double-zeta basis sets (cc-pVDZ) are used. PSI4 1.0 is selected to perform SAPT0 calculations [18]. More computational details are described in Supporting Information.

3. Results and discussion

As spun CNT fibers showed complexed hierarchical structures with voids which act as a defect site impeding efficient load and electron transfer and thus diminishing mechanical and electrical properties of CNT fibers (Fig. 1a) [7]. As a result, their diameter, tensile strength, modulus, specific strength and electrical conductivity were measured to be 72.6 μm (Fig. 2a), 72 MPa, 2 GPa, 0.42 N tex^{-1} and 968 S cm^{-1}, respectively (Fig. 2b, c, d, e). To enhance mechanical and electrical properties, the voids in CNT fibers should be filled with adhesive, strong and electrically conductive materials [12].

DFT calculation has been carried out for the systematic design of interface between RF resin and CNT fiber. RF resin is mainly bound to SWCNT via dispersion interaction and small contribution from an electrostatic term (Fig. 3a), and binding energy is predicted to be 21.9 kcal mol^{-1}, which is higher that the interaction of SWCNT and polydopamine repeating unit by ~1 kcal mol^{-1} (Fig. 3e and see Fig. S1 for dopamine on SWCNT). CTAB, a surfactant to improve surface-coating efficiency of RF resin on various nanomaterials [20], is tested as a potential additive to lead further increase in interfacial binding energy. The individual interaction for CTAB-SWCNT and CTAB-RF resin is examined to understand whole complex binding energy. Long carbon chain is linearly aligned on SWCNT to maximize dispersion interaction

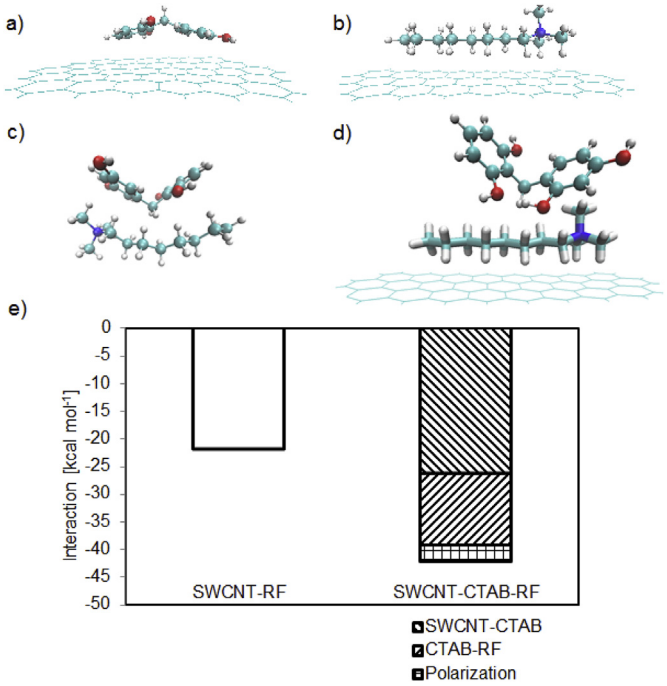

Fig. 3. (a) Illustration of RF resin on CNT, (b) CTAB on SWCNT, (c) RF resin with CTAB, (d) RF resin on SWCNT with CTAB and (e) Interaction energy of SWCNT-RF resin and SWCNT-CTAB-RF resin. Color scheme: hydrogen, white; carbon, cyan; nitrogen, blue; oxygen, red. (For interpretation of the references to colour in this figure legend, the reader is referred to the Web version of this article.)

and the most positive charged part of ammonium is bound to SWCNT via cation-π complex interaction (Fig. 3b). The amount of interaction is evaluated to be $-26.3\,kcal\,mol^{-1}$ ('SWCNT-CTAB' in Fig. 3e). The cationic ammonium in CTAB strongly interacts with the electron-rich benzene part of RF resin with being $12.9\,kcal\,mol^{-1}$ favored (Fig. 3c and 'CTAB-RF' in Fig. 3e). Investigation of whole system, SWCNT-CTAB-RF resin (Fig. 3d), shows that synergistic interaction owing to charge polarization upon CTAB insertion increases the total interaction energy up to $42.1\,kcal\,mol^{-1}$ ('Polarization' in Fig. 3e). This DFT calculation suggested RF resin can be efficiently infiltrated into CNT fibers in the presence of CTAB and result in their considerable reinforcement by the densification effect.

The polymerization of RF resin was applied to CNT fibers for the infiltration in presence of CTAB to reinforce their mechanical and electrical properties (for the analysis of RF resin polymerization with CTAB, see Fig. S2). The tensile strength and modulus of pristine CNT fiber increased to 155 MPa and 9 GPa, while its specific strength was not affected ($0.42\,N\,tex^{-1}$) by RF polymerization for 10 min (Fig. S3). After 3 h polymerization, the C-RF resin weight fraction of C-RF@CNT fibers was 65% and their tensile strength, modulus and specific tensile strength of C-RF@CNT fibers reached to plateau (244 MPa, 14 GPa and $0.56\,N\,tex^{-1}$) (Fig. 4a, b, c and Fig. S3) while electrical conductivity increased to $1741\,S\,cm^{-1}$ (Fig. 4d). The enhanced specific tensile strength by C-RF resin infiltration implied the load transfer efficiency between C-RF resin and CNT fibers was significantly improved to overwhelm the increased weight by C-RF resin infiltration. The infiltration of C-RF resin was confirmed with SEM images of C-RF@CNT fibers showing well connected structures of CNT bundles (Fig. 4e). The improved mechanical and electrical properties of C-RF@CNT fibers compared to pristine CNT fibers concurred with DFT simulation. It is noteworthy the tensile strength, modulus, specific tensile strength and electrical conductivity of CNT fibers were highly enhanced without thermal carbonization.

For further reinforcement, thermal carbonization processes of C-RF were investigated (Fig. S4). The optimized stabilization and carbonization processes were then applied to C-RF@CNT fibers. After the stabilization and carbonization, the diameter of C-RF@CNT fiber greatly decreased from 64.6 to 32.7 μm (Fig. 5a). This decrease implied the C-RF@CNT fiber was further densified by the stabilization and carbonization. SEM images showed that the carbonized C-RF@CNT (CRF@CNT) fiber possessed highly connected structures (Fig. 5a) compared to pristine CNT and C-RF@CNT fibers (Fig. 2a and b and Fig. 4e). Chemical structure changes of CNT fibers during the C-RF infiltration and carbonization were investigated by using XPS and Raman spectroscopies. The C/O ratio of pristine CNT fibers was measured to be 9.95 and this value decreased to 7.78 by C-RF resin infiltration because of the large amount of phenol groups (Fig. S5a). After the carbonization, the C/O ratio of C-RF@CNT fibers increased to 10.07 higher than that of pristine CNT fibers (Fig. S5a). Raman spectra of CNT, C-RF@CNT and CRF@CNT exhibited the typical G- and D-peaks (Fig. S5b) [21]. The G and D-peaks intensity ratio (I_G/I_D) of CNT fibers was 17.4 (Fig. S5b). This value decreased to 9.5 by RF infiltration and this decrease might be attributed to the strong interaction between C-RF resin and CNT fibers. The I_G/I_D of C-RF@CNT fibers was further lowered to 5.3 (Fig. S5b) by thermal stabilization and carbonization. This decreasing I_G/I_D was attributed to the evolution of D-peak which originated from the carbonization of C-RF resin (Fig. S4b). Those spectroscopic analyses confirmed that the carbonization process of C-RF resin was successfully adopted to C-RF@CNT fibers.

The influence of carbonization on the mechanical and electrical

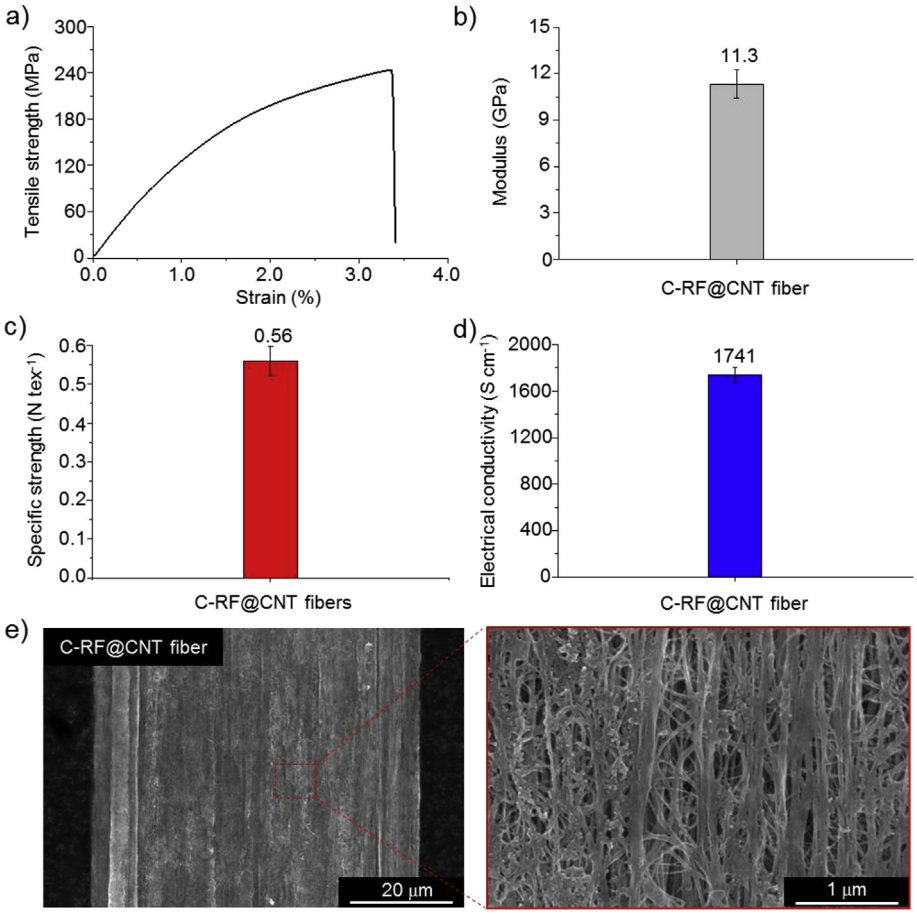

Fig. 4. (a) SEM images, (b) stress and strain curve, (c) modulus, (d) specific tensile strength and (e) electrical conductivity of C-RF@CNT fibers.

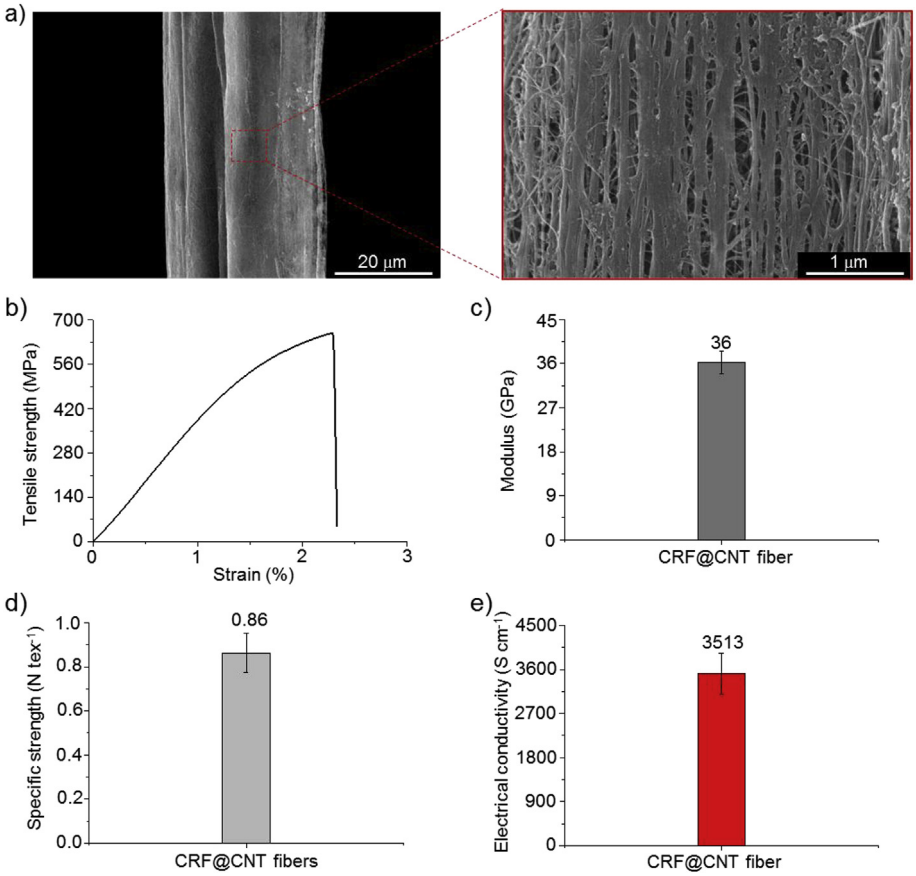

Fig. 5. (a) SEM images of CRF@CNT fibers with different magnification. b) stress and strain curve, (c) modulus, (d) specific tensile strength and (e) electrical conductivity of CRF@CNT fibers.

properties of C-RF@CNT fibers was explored to confirm the reinforcement of CNT fibers by C-RF infiltration and followed by carbonization. Compared to the C-RF@CNT fibers, the CRF weight fraction of CRF@CNT fibers decreased to 56% and they exhibited considerably increased tensile strength, modulus and specific strength from 253 MPa, 11 GPa and 0.65 N tex^{-1} to 610 MPa, 36 GPa and 0.86 N tex^{-1}, respectively (Fig. 5b, c, d). These results indicated that the mechanical properties of C-RF@CNT fibers were greatly improved by the thermal stabilization and carbonization processes. By contrast, the thermal treatment of pristine CNT fibers under the equal condition did not induce significant structural changes and mechanical reinforcement of CNT fibers (see Figs. S7 and S8 for the detailed information). This control experiment further confirmed the densification and mechanical reinforcement of CNT fibers originated from the carbonization of infiltrated C-RF resin.

The electrical conductivity of C-RF@CNT fibers also increased from 1741 to 3513 S cm^{-1} (Fig. 5e). These results clearly proved that the C-RF resin infiltration, thermal stabilization and carbonization processes resulted in the substantial enhancement of both mechanical and electrical properties of CNT fibers.

Fracture analyses of pristine CNT, C-RF@CNT and CRF@CNT fibers were carried out to verify reinforcement mechanism of CNT fibers. Characteristic hairy-type failure was observed from CNT fiber because the failure occurs by sliding of individual CNT consisting of CNT fiber when the strain force is over the friction force (Fig. 6a) [14]. This sliding and failure started at a void and/or at the end of CNT where the applied stress was concentrated. C-RF@CNT fiber exhibited less hairy-type structures at its fracture surface which was attributed to strengthened interaction and suppressed sliding between individual CNT by C-RF resin (Fig. 6a). CRF@CNT fiber presented almost no hairy-type structure at its failure surface (Fig. 6a) and this result suggested the interaction between carbonized C-RF resin and CNT fiber was stronger than that between individual CNT. The cross-sectional SEM and polarized Raman analyses were performed to further elucidate the reinforcement mechanism of CNT fibers. The cross-sectional SEM images of C-RF@CNT fiber showed the voids of CNT fibers were filled with C-RF resin, and it was further densified by thermal carbonization accompanied with degasification (Fig. 6b). Therefore, the density of CNT fibers sequentially increased by the order of CNT, C-RF@CNT and CRF@CNT fibers (Fig. 6b). This tendency implied the C-RF resin infiltration lead to the densification of CNT fibers based on the attractive interaction between C-RF resin and CNT and the CRF resin also provided the comparable attractive interaction with CNT. This interpretation can be further supported by the sequentially decreased cross-sectional areas of CNT fibers (Figs. S6a and b) accompanied with the sequential increase of their load values (Fig. S6c) by the C-RF resin infiltration and its thermal carbonization. Taken together, it was clearly revealed that the present reinforcement of mechanical properties of CNT fibers did not simply originate from the decrease of cross-sectional area by densification induced by thermal treatments, but it was derived from the combinatorial effect of the improved load bearing capacity and densification of CNT fibers by infiltration of C-RF resin and its conversion into carbonized structures. In the case of electrical conductivity, the electrical resistance of CNT fibers increased from 0.183 ± 0.001 kΩ to 0.206 ± 0.007 kΩ for C-RF@CNT fibers and 0.222 ± 0.028 kΩ for CRF@CNT fibers, respectively. However, the electrical conductivity of CNT fibers increased by the C-RF infiltration and subsequent thermal carbonization owing the considerable decrease of their cross-sectional area (Figs. S6a and b). Therefore, the enhanced electrical conductivity of CNT fibers was dominantly attributed to the densification effect.

Then, the ratio of the Raman intensity of CNT, C-RF@CNT and

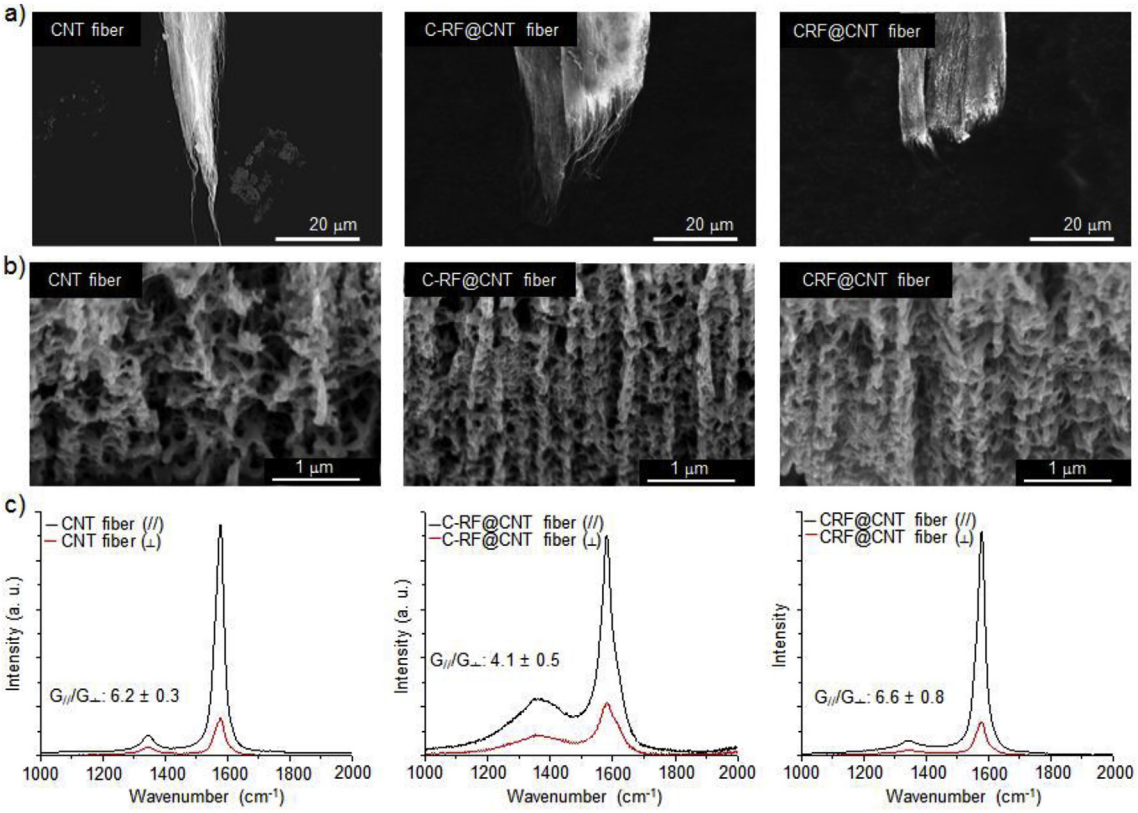

Fig. 6. (a) Fractography SEM images, (b) cross-sectional SEM images and (c) polarized Raman spectra of CNT, C-RF@CNT and CRF@CNT fibers.

CRF@CNT fibers depending on the parallel (I_0°) and perpendicular polarization (I_{90}°) were analyzed to explore changes of internal alignment of CNT fibers. The I_0°/I_{90}° ratio increased with the alignment in CNT fiber [22]. The I_0°/I_{90}° ratio of pristine CNT fibers was 6.16 and it decreased to 4.12 by C-RF infiltration (Fig. 6c). This decrease suggested the RF resin infiltration induced the slight collapse of alignment. However, the I_0°/I_{90}° ratio of CRF@CNT fibers increased to 6.64 slightly higher than that of pristine CNT fibers by the thermal stabilization and carbonization (Fig. 6c). Those results verified that the C-RF resin infiltration, subsequent thermal stabilization and carbonization resulted in high degree of densification as well as alignment of CNT fibers.

4. Conclusion

In summary, we demonstrated an efficient enhancement strategy for both mechanical and electrical properties of CNT fibers by the sequential processes such as RF resin infiltration, thermal stabilization and carbonization. It was proved by DFT calculation that C-RF resin and CNT fiber were strongly interacted each other. As a result, RF resin was infiltrated into CNT fibers in the presence of CTAB and thus the tensile strength, modulus, specific tensile strength and electrical conductivity of CNT fibers were respectively improved from 71 MPa, 2 GPa, 0.33 N tex^{-1} and 968 S cm^{-1} to 610 MPa, 36 GPa, 0.88 N tex^{-1} and 3513 S cm^{-1} by the improved load and electron transfer, densification and alignment effect. This strategy will be a practical and important tool to develop high-performance carbon nanomaterial-based fibers for automobile, defense and aerospace industries due to its simplicity, cost-effectiveness and high efficiency.

Acknowledgement

This research was financially supported by grants from the Korea Institute of Science and Technology (KIST) Open Research Program (ORP) and Nano·Material Technology Development Program through the National Research Foundation of Korea funded by the Ministry of Science, ICT and Future Planning (2016M3A7B4027223) and (2016M3A7B4905619).

Appendix A. Supplementary data

Supplementary data to this article can be found online at https://doi.org/10.1016/j.compositesb.2018.12.132.

References

[1] Peng B, Locascio M, Zapol P, Li S, Mielke SL, Schatz GC, et al. Measurements of near-ultimate strength for multiwalled carbon nanotubes and irradiation-induced crosslinking improvements. Nat Nanotechnol 2008;3:626–31.
[2] Ebbesen TW, Lezec HJ, Hiura H, Bennett JW, Ghaemi HF, Thio T. Electrical conductivity of individual carbon nanotube. Nature 1996;382:54–6.
[3] Zhang M, Atkinson KR, Baughman RH. Multifunctional carbon nanotube yarns by downsizing an ancient technology. Science 2004;306:1358–61.
[4] Behabtu N, Young CC, Tsentalovich DE, Kleinerman O, Wang X, Ma AW, et al. Strong, light, multifunctional fibers of carbon nanotubes with ultrahigh conductivity. Science 2013;339:182–6.
[5] Li YL, Kinloch IA, Windle AH. Direct spinning of carbon nanotube fibers from chemical vapor deposition synthesis. Science 2004;304:276–8.
[6] Koziol K, Vilatela J, Moisala A, Motta M, Cunniff P, Sennett M, Windle A. High-performance carbon nanotube fiber. Science 2007;318:1892–4.
[7] Xu W, Chen Y, Zhan H, Wang JN. High-strength carbon nanotube film from improving alignment and densification. Nano Lett 2016;16:946–52.
[8] Qiu J, Terrones J, Vilatela JJ, Vickers ME, Elliott JA, Windle AH. Liquid infiltration into carbon nanotube fibers: effect on structure and electrical properties. ACS Nano 2013;7:8412–22.
[9] Jung Y, Kim T, Park CR. Effect of polymer infiltration on structure and properties of carbon nanotube yarns. Carbon 2015;88:60–9.
[10] Lee J, Kim T, Jung Y, Jung K, Park J, Lee DM, et al. High-strength carbon nanotube/carbon composite fibers via chemical vapor infiltration. Nanoscale 2016;8:18972–9.
[11] Liu K, Sun Y, Lin X, Zhou R, Wang J, Fan S, et al. Scratch-resistant, highly conductive, and high-strength carbon nanotube-based composite yarns. ACS Nano 2010;4:5827–34.
[12] Allen R, Pan L, Fuller GG, Bao Z. Using in-situ polymerization of conductive

polymers to enhance the electrical properties of solution-processed carbon nanotube films and fibers. ACS Appl Mater Interfaces 2014;6:9966–74.
[13] Ryu S, Chou JB, Lee K, Lee D, Hong SH, Zhao R, et al. Direct insulation-to-conduction transformation of adhesive catecholamine for simultaneous increases of electrical conductivity and mechanical strength of CNT fibers. Adv Mater 2015;27:3250–5.
[14] Youn DH, Patterson NA, Park H, Heller A, Mullins CB. Facile synthesis of Ge/N-doped carbon spheres with varying nitrogen content for lithium ion battery anodes. ACS Appl Mater Interfaces 2016;8:27788–94.
[15] Chai JD, Head – Gordon M. Phys. Chem. Long-range corrected hybrid density functionals with damped atom-atom dispersion corrections. Chem Phys 2008;10:6615–20.
[16] Hasanzade Z, Raissi H. Solvent/co-solvent effects on the electronic properties and adsorption mechanism of anticancer drug Thioguanine on Graphene oxide surface as a nanocarrier: density functional theory investigation and a molecular dynamics. Appl Surf Sci 2017;422:1030–41.
[17] Hohenstein EG, Sherill CD. Density fitting and Cholesky decomposition approximations in symmetry-adapted perturbation theory: implementation and application to probe the nature of π-π interactions in linear acenes. J Chem Phys 2010;132:184111.
[18] Turney JM, Simmonett AC, Parrish RM, Hohenstein EG, Evangelista FA, Fermann JT, et al. Psi4: an open-source ab initio electronic structure program. Wiley Interdiscip. Rev. Comput. Mol. Sci. 2012;2:556–65.
[20] Li N, Zhang Q, Liu J, Joo J, Lee A, Gan Y, et al. Sol-gel coating of inorganic nanostructures with resorcinol-formaldehyde resin. Chem Commun 2013;49:5135–7.
[21] Pimenta MA, Dresselhaus G, Dresselhaus MS, Cançado LG, Jorio A, Saito R. Studying disorder in graphite-based systems by Raman spectroscopy. Phys Chem Chem Phys 2007;9:1276–91.
[22] Zhou J, Sun G, Zhan Z, An J, Zhang Y, Zhang Y, et al. Polarization behaviors of twisted carbon nanotube fibers. J Raman Spectrosc 2012;43:1221–6.